Silicon (2022) 14:5661–5671
https://doi.org/10.1007/s12633-021-01347-2

ORIGINAL PAPER

Synthesis of Pb_3O_4-SiO_2-ZnO-WO_3 Glasses and their Fundamental Properties for Gamma Shielding Applications

Sultan Alomairy[1] · Z. A. Alrowaili[2] · Imen Kebaili[3,4] · E. A. Abdel Wahab[5] · C. Mutuwong[6] · M. S. Al-Buriahi[7] · Kh. S. Shaaban[8]

Received: 18 July 2021 / Accepted: 23 August 2021 / Published online: 2 September 2021

Abstract

Zinc lead silicate glass system contains different amount of WO_3 were fabricated using the classical melt-quench technique. The nature of the samples was investigated using X-ray diffraction. The ultrasonic velocities and elastic moduli were tested experimentally after that the results were compared by using the theoretical consideration. With increasing the WO_3 content, decreasing the molar volume causes a decrease in the inter-ionic distance R_i. The FLUKA code were used to estimate the main attenuation considerations mass attenuation coefficients (MAC) and linear attenuation coefficients (LAC). The LAC increment from 0.728 cm-1 to 0.856 cm^{-1} as the WO_3 concentration increment from 0 to 5 mol%, resulting in high shielding performance for G5. The dose rate at energy of 0.6 MeV with the G5 sample found to be declines from 2.35×10^7 R/h at 1 mm to 4.71×10^6 R/h at 4 mm. The values of mean free path (MFP) and the half value layer (HVL) are smaller than those of the traditional photon shields signifying that the fabricated samples (particularly G5) have interesting shielding characteristics to be used in applications involving x/gamma rays.

Keywords Silicate glass · micro-hardness · XRD · Structural properties · Gamma shielding

1 Introduction

In the various application of glass materials, silicate glass plays an important role due to their unique features like high solubility, high non-linear optical factors, good mechanical moduli, small thermal expansion, and excellent glass-forming domain [1–8]. Moreover, these glasses can be considered as transition metal ion (TMi) to manufacture super-effective optical and luminescence mechanisms. Furthermore, doping by (TM) with various valences gives the silicate glasses a broad range of scientific and technological importance to use for many applications in various fields [9–17].

In the field of optoelectronic tools, screen reflection, thermal and mechanical instruments, attenuation protecting, etc., glasses based on weighty metal oxides (WMO) as Pb_3O_4, Bi_2O_3, WO_3 and Y_2O_3 have extensive applications [18–29]. WMO glasses extremely have density therefore its superior gamma-ray shielding attributes. A great candidate for γ-ray shielding purpose has been found to be lead containing silicate glasses. Pb_3O_4 are identified as intermediary oxides, or provisional glass network modifiers. Subsequently, the percentage of the oxide in glass play an important role, it may be

✉ Kh. S. Shaaban
khamies1078@yahoo.com

1 Department of Physics, College of Science, Taif University, P.O.Box 11099, Taif 21944, Saudi Arabia

2 Physics department, College of Science, Jouf University, P.O.Box: 2014, Sakaka, Saudi Arabia

3 Department of Physics, Faculty of Science, King Khalid University, P.O. Box 9004, Abha, Saudi Arabia

4 Laboratoire de Physique Appliquée, Groupe des Matériaux Luminescents, Université de Sfax, Faculté des Sciences de Sfax, BP 1171, 3000 Sfax, Tunisia

5 Physics Department, Faculty of Science, Assiut University, P.O. Box 71524, Assiut, Egypt

6 Department of Physics, Ubon Ratchathani University, Ubon Ratchathani, Thailand

7 Department of Physics, Sakarya University, Sakarya, Turkey

8 Chemistry Department, Faculty of Science, Al-Azhar University, P.O. Box 71524, Assiut, Egypt

Table 1 Chemical formula of fabricated glasses (mol. %)

Sample Name	SiO_2 mol.%	Pb_3O_4	ZnO	WO_3
G1	60	35	5	0
G2	60	35	4	1
G3	60	35	2	3
G4	60	35	1	4
G5	60	35	0	5

act as network former or network modifier. Once its concentration higher than 30 mol%, Pb_3O_4 acts as both network former and network modifier in some silicate glasses. As Pb_3O_4 modifies the network of silicate glasses, the structural units of silicate may be interacted with the structural unit of lead (PbO_4) strongly. Tungstate glasses is classified as non-traditional glasses. In its compounds, WO_3, can explore 6 ionization states: from zero (0) to six (+6). It is founded in form W^{+3}, W^{+4}, W^{+5} and W^{+6} at many prepared and published glasses systems. The emergence of WO_3 into the network enhanced many characteristics properties of the manufacture systems [30–32].

On The Other Hand, some (WMi) or (TMi) holding glasses demonstrate protecting behavior toward more successive γ-rays. Several research on radiation effect on various doped glasses with different transition metal ions (TMi) have recently been developed by El Batal et al. [33, 34]. Among the disguised objectives of several researchers, the requirements of substances that can perform a dual function across the last period can be considered. Considerable numbers of glass research laboratories are increasing daily to develop superior and useful features to use in protection purpose. These glasses are applied in advanced optical tools and in radiation shielding where radiation safety is needed.

The glass under studied has grown to be preferred replacement for concrete shielding due to its extraordinary features such as stiffness, and mechanical potency, likewise these glasses, have clarity and mechanical strength. The main objective of the paper under investigation is to prepare, recognize the attenuation impact of zinc lead silicate glasses containing various quantities of W^{3+} and determine of its mechanical characteristics.

2 Material Ad Methods

Table 1 explore the content of fabricated glasses [35]. SiO_2, Pb_3O_4, ZnO and WO_3 are the primary raw materials for getting these samples. Original materials that were purchased from Sigma-Aldrich Company. The blend materials were grinding continually to acquire a fine powder. To evaporate H_2O and other volatile compounds or elements, the start materials were heated to 950 K for 30 min., then raised for 90 min to 1350 K. The samples were annealed at 700 K for 3 h to reduce internal stresses.

The nature of fabricated samples were investigated with (A Philips X-ray diffractometer PW/1710) and its amorphous state is confirmed. Density of the glasses determined by Archimedes' code $\rho = \rho_0\left(\frac{M_a}{M_o - M_1}\right)$ [35]. The volume of molar(V_m) evaluated using $V_m = \frac{M_a}{\rho}$.

Using the pulse-echo technique, the ultrasonic velocities, longitudinal (v_L) and shear (v_T), at ambient temperature were evaluated, by KARL DEUTSCH Echograph model 1085 (a digital ultrasonic flaw detector) functioning at 4 MHz with error ± 10 m s^{-1}. Farther the density, the speeds have been used to estimate elastic moduli. longitudinal waves $L = \rho v_L^2$, transverse waves $G = \rho v_T^2$, bulk modulus $K = L - \left(\frac{4}{3}\right)G$ finally, Young's modulus $Y = (1 + \sigma)2G$ [15–32].

By theoretical equation the elastic moduli of the samples were determined [36, 37] depend on packing density $Vi = \left(\frac{3\pi}{4}\right)N_A\ (m\mathrm{R}^3 + n\ \mathrm{R}_\mathrm{O}^3)\ m^3/mol$, and dissociation energy $Gi = \left(\frac{1}{V_m}\right)\sum_i G_i\ X_i$, where the ionic radii of metallic and oxygen Pauling are R_m and R_O respectively. Longitudinal waves $L = K + \left(\frac{4}{3}\right)G$, transverse waves $G = 30*\left(\frac{V_i^2 G_i}{V_i}\right)$ Young's modulus $Y = 8.36 V_i G_i$, bulk modulus $K = 10 V_i^2 G_i$. Poission's ratio $\sigma = \frac{1}{2} - \left(\frac{1}{7.2 * Vi}\right)$. Acoustic Impedance; $Z = v_L \rho$. Micro Hardness; $\mathrm{H} = (1 - 2\sigma)\ \frac{\mathrm{Y}}{6(1+\sigma)}$. Debye Temperature: $\theta_D = \frac{h}{k}\left(\frac{9N_A}{4\pi\ V_m}\right)^{\frac{1}{3}} M_s$, Where N_A is the number of Avogadro, Planck constant *is* h and Boltzmann constants is k.

Average velocities $M_s = \frac{1}{3}\left(\frac{\frac{2}{v_t^3} + \frac{1}{v_l^3}}{}\right)^{\frac{1}{3}}$, Thermal coefficient of expansion $\alpha_P =$ $= 23.2\ (v_L - 0.57457)$, the molar volume

Fig. 1 Photographic of Pb_3O_4-SiO_2-ZnO-WO_3 glasses

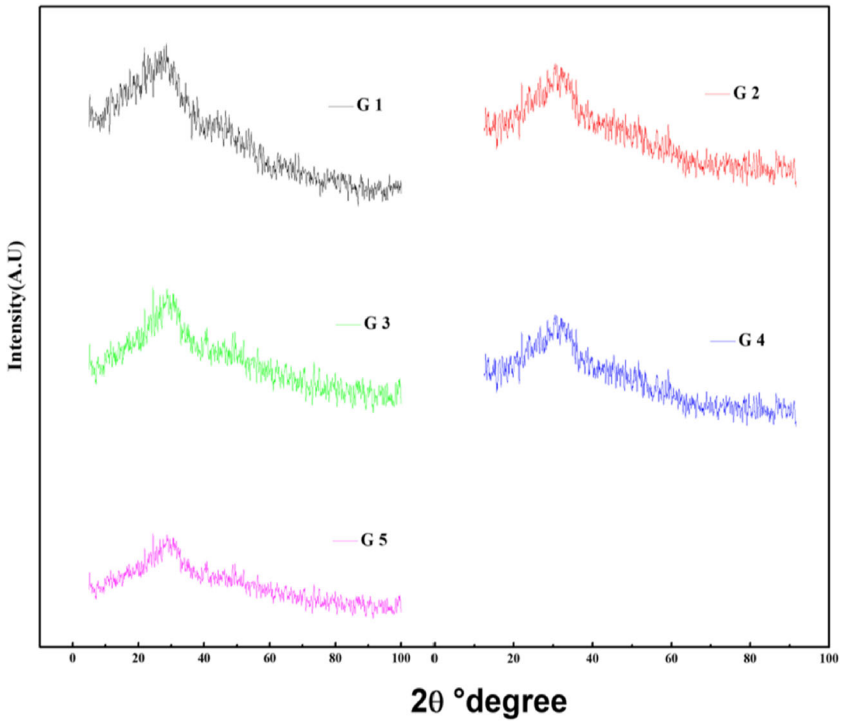

Fig. 2 XRD of Pb_3O_4-SiO_2-ZnO-WO_3 glasses

of oxygen estimated by $V_o = \left(\frac{M}{\rho}\right)\left(\frac{1}{\sum xini}\right)$ and the oxygen packing density as $OPD = \left(\frac{1000\ C}{Vm}\right)\left(\frac{Mol}{L}\right)$.

Monte Carlo technique is a simulation process for a full description of any experiment in a software environment. In the present study, several Monte Carlo simulations were applied via FLUKA code which is a powerful platform to handle the propagation of radiation (e.g. photons) for a large energy range reaching several hundred MeV [38]. In fact, the FLUKA code is mainly designed to generate the events (collisions) of hadrons in high energy physics. However, since 15 years FLUKA code is used for electromagnetic interactions with high accuracy for estimating the cross sections for photons and electrons. For the present work, we used FLUKA2005.6 version that have a huge library for the photon interactions including coherent process, pair production, and photoelectric effect. Moreover, it is worth mention that different Monte Carlo platforms such as PHITS, Geant4, and MCNP approved their successes to evaluate the photon shielding parameters for several studies [39–45].

3 Results and Discussion

Fig. 1 explores the photographic of arranged glasses. As illustrated in Fig. 2, no distinct lines, no strong peaks, are presented of the XRD shapes, this if indicating that the prepared glass has a high degree of amorphous state. Tungsten ion concentration was calculated as:

$$\mathrm{W}i = \left(\frac{6.023 \times 10^{23} x\ mol\ fraction\ of\ cation \times valency\ of\ cation}{Vm}\right) \quad (1)$$

It is increases with tungsten ion increased this is dependent on the reduction of *Vm*. Computed inter-ionic distance as.

$$R_i = \left(\frac{1}{\text{Concentration of W}}\right)^{\frac{1}{3}} \quad (2)$$

Radius was established as polaron r_p and internuclear r_i, was calculated as: $rp = \frac{1}{2}\ \left(\frac{\pi}{6N}\right)^{\frac{1}{3}}, ri = \left(\frac{1}{N}\right)^{\frac{1}{3}}$. W – W separation ($d_{W\text{-}W}$) computed as:$(dW{-}W) = \left(\frac{V_m^B}{N}\right)^{\frac{1}{3}}$ and $V_m^B = \frac{Vm}{2(1-2Xn)}$. As a result of the decrease in *Vm*, these have been observed that these characteristics decrease with tungsten. For BO or NBO linking verification, the average number that has been coordinated is a considerable factor and is calculated as $m = \sum n_{ci} X_i$ where $n_{ci}$is the cation coordination. Calculating the number per unit of bonds is estimated as $n_b = \frac{N_A}{\sum n_{ci} X_i} V_m$. These characteristics have been noted to be increased

Table 2 Physical properties of fabricated glasses

parameters	G 1	G 2	G 3	G 4	G 5
(N_i) (10^{21} ions/cm^3)	–	0.836	2.52	3.5	4.7
Ri (A°)	–	10.8	7.47	6.7	6.08
ri (Å)	–	12.5	8.7	7.77	7.08
r_p (Å)	–	3.6	2.5	2.23	2.03
W-W separation($d_{w\text{-}w}$), nm	0.597	0.591	0.586	0.577	0.562
(m)	3.9	3.94	3.98	4.06	4.1
n_b (10^{28} m^{-3})	5.32	5.48	5.62	5.92	6.39

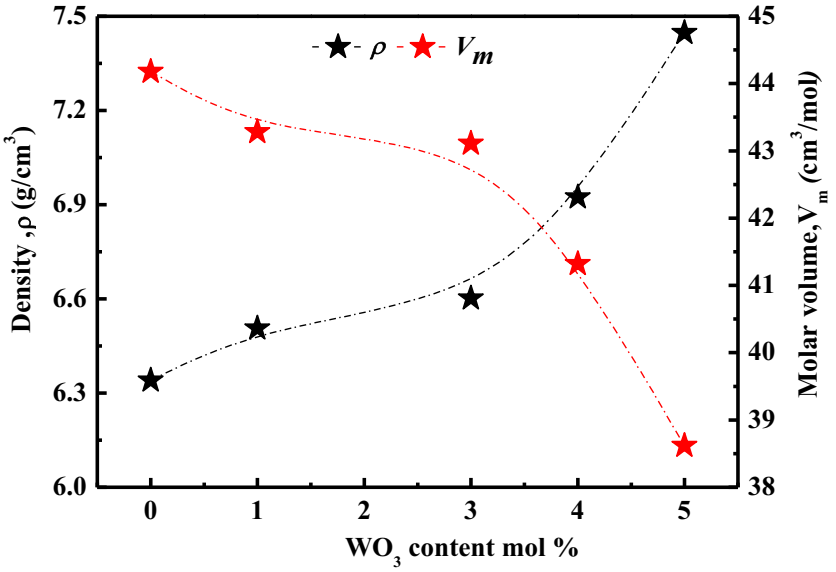

Fig. 3 ρ & V_m *of* Pb_3O_4-SiO_2-ZnO-WO_3 glasses

with an increase in tungsten oxide concentration. All these characteristics, as shown in Table 2.

Figure 3 depicts the changes in the glass system's *Vm* and density. The densities of these samples increased as the WO_3 content increased, while *Vm* reduced. Because of the variation in molecular quantities between ZnO and WO_3 [81.389 & 231.838], the density increased. With increasing tungsten concentration, decreased molar volume values are reported in the present study. The network is therefore more compact, and the glass matrices have increased connectivity. The variations in V_o and *OPD* demonstrated in Fig. 4. The values of V_o have been observed to decrease while the *OPD* has been enhanced. These results pointed to an increase in the number of oxygen bridges (BO) due to the decrease in *Vm*.

The velocity of prepared glasses with varying quantities of tungsten oxide has been exemplified in Fig. 5. As shown in Table 3, both velocities (v_L and v_T) were improved with an increase in WO_3 and (v_L) values higher than (v_T). The expansion in the evaluated ultrasonic velocity may be clarified by considering the following variables:

(i) Increasing WO_3 will improve the amorphous network by increasing average coordination number in structural unit.
(ii) Consequently, there was an increased polymerization of the glass coordination number, cross-link density and linkage within the glass network.
(iii) Because increasing in internal strength, the speeds were increased.

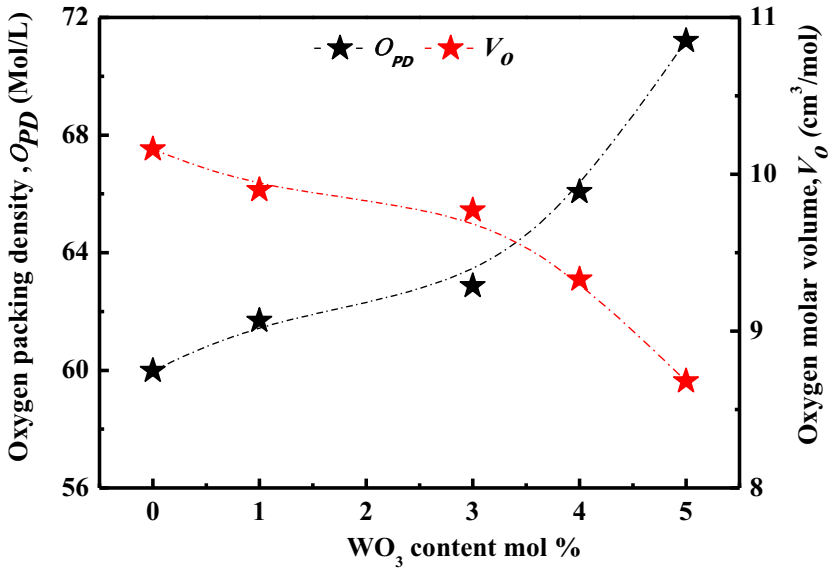

Fig. 4 O_{PD} & V_o *of* Pb_3O_4-SiO_2-ZnO-WO_3 glasses

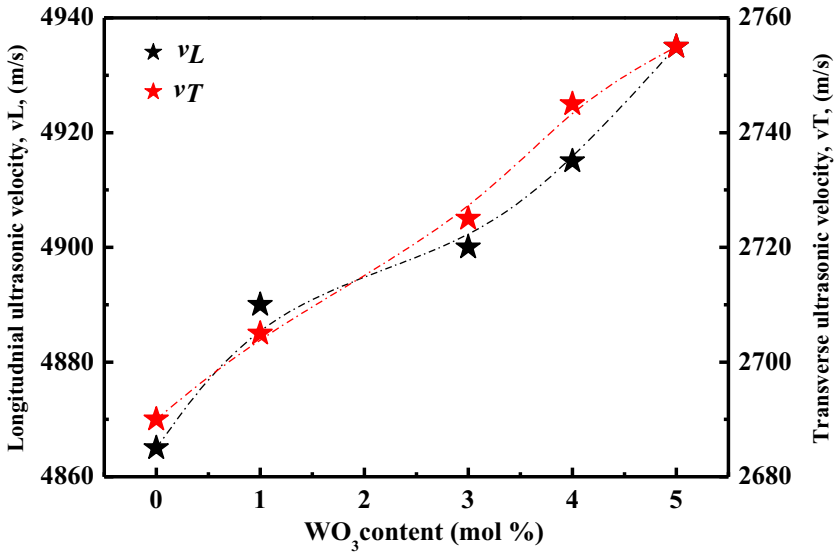

Fig. 5 $V_{L\&}$ V_T of Pb_3O_4-SiO_2-ZnO-WO_3 glasses

Table 3 The values of $v_{L,}$ v_T and elastic moduli of fabricated glasses

Samples name	v_L $(m.s^{-1})$	v_T	L (GPa)	G	K	Y	L_M	G_M	K_M	Y_M
G 1	4865	2690	150.06	45.88	88.89	117.43	41.5	14.6	20.2	39.3
G 2	4890	2705	155.57	47.60	92.10	121.82	43	15.5	20.6	40.7
G 3	4900	2725	158.51	49.02	93.15	125.12	44.5	16.4	21.1	41.9
G 4	4915	2745	167.26	52.17	97.70	132.87	47.4	18.3	21.8	44.4
G 5	4935	2755	181.37	56.52	106.00	143.98	52	21.4	23	48.1

Elastic modules were evaluated experimentally and determined theoretically, for fabricated samples and exemplified in Figs. 6 and 7. The elastic moduli act in the same way that velocities do, as shown in Figs. 6 and 7 i.e., it is determined by the nature of the glass's bonds and the cross-link density. By increasing WO_3, values of elastic moduli show an increasing tendency. The number of coordinates has increased in tandem with the growth in elastic modules and heat of formation of W– O (653.1 $KJmol^{-1}$) is higher than Zn – O (284.1 $KJmol^{-1}$), which promotes the

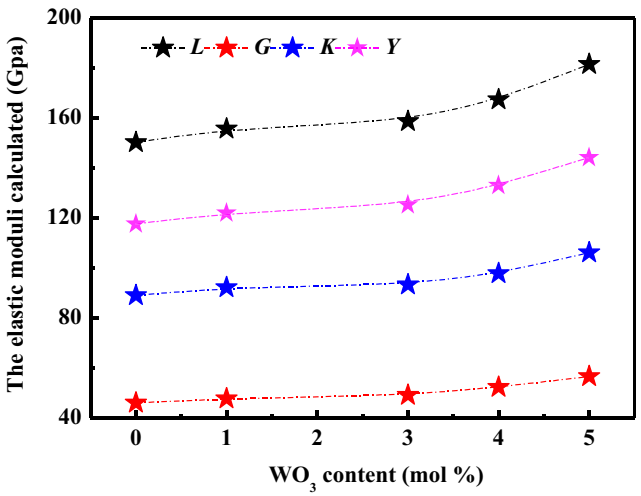

Fig. 6 Experimental elastic modules of prepared glasses with varying quantities of WO_3

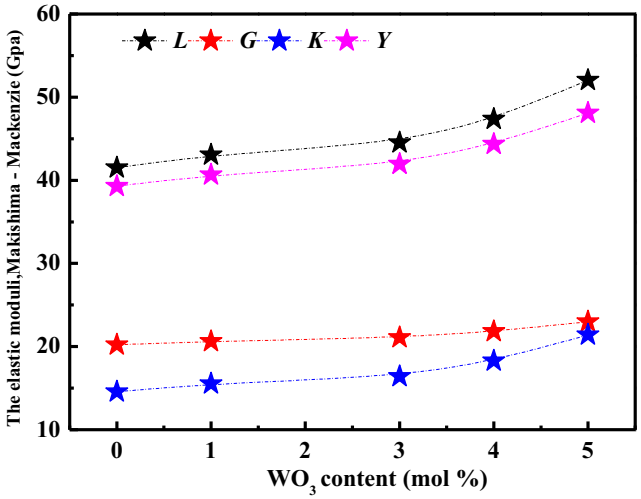

Fig. 7 Theoretical elastic modules of prepared glasses with varying quantities of WO_3

Table 4 Values of, (*Vi*), (*Gi*), (α_P), (Z), (θ_D), (O_{PD}), (V_o), (*H*) and, (T_s) of the glasses under investigation

Samples name/parameters	$V_i \times 10^{-6}$, (m^3)	Gi, (kcal/kJ)	α_p, (K^{-1})	*d*	σ	$Zx10^7$ ($kg.m^{-2}.s^{-1}$)	θ_D, (K)	O_{PD}, (mol/L)	V_o, (cm^3/mol)	H, (GPa)	T_s, (K)
G 1	0.31	15.16	112,854.67	2.06	0.052	3.08	310.76	59.99	10.16	6.73	1539.5
G 2	0.32	15.22	113,434.67	2.07	0.065	3.18	315.3	61.69	9.9	6.997	1561.2
G 3	0.33	15.34	113,666.67	2.11	0.075	3.235	319.3	62.87	9.77	7.317	1591.2
G 4	0.344	15.41	114,014.67	2.13	0.097	3.4	326.77	66.07	9.33	7.88	1620
G 5	0.372	15.47	114,478.67	2.133	0.127	3.675	336.14	71.21	8.68	8.53	1635.4

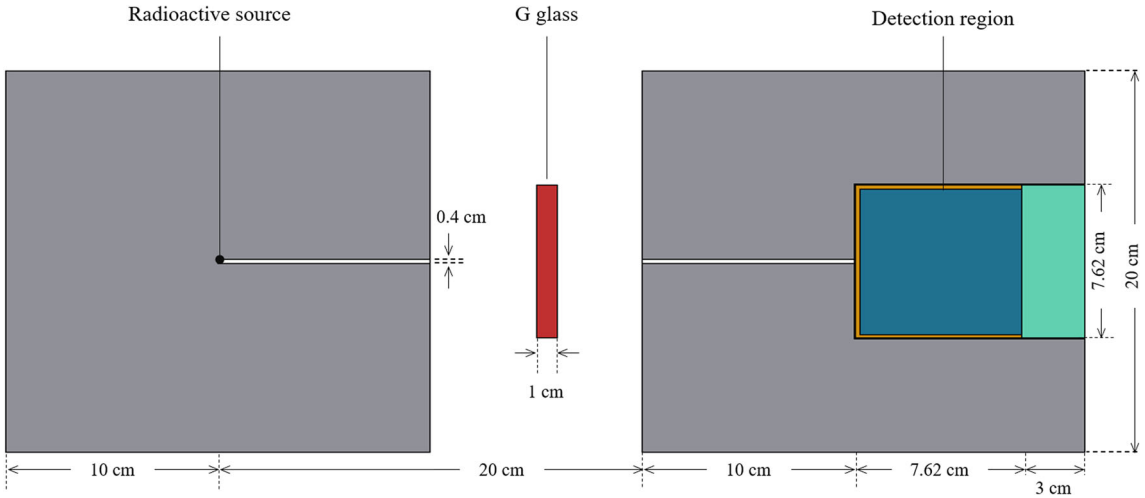

Fig. 8 The present work used the FLUKA code

development of tungstate glasses rather than zincate. Elastic modules exposed in Table 4.

Figure 8 illustrates a schematic representation for the well-known experiment setup namely, the narrow beam transmission experiment. The geometry of such experiment is an essential block to study and understand the radiation interaction (especially x/gamma rays) with materials. In the present work, we draw this geometry by using FLUKA code. The main attenuation parameters: mass and linear coefficients, give a full understanding of photon propagation through mass/linear thickness of an absorbing target. Both MAC and LAC were obtained utilizing several simulations for every energy by FLUKA code. The simulations outcomes of these factors were plotted in Fig. 9. Both μ/ρ and μ have similar variation with

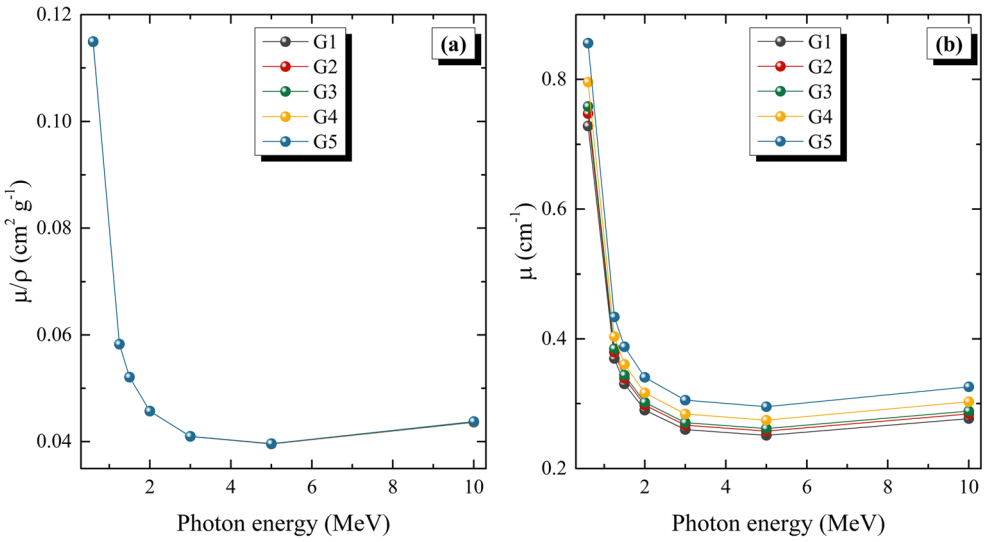

Fig. 9 LAC for the SiO_2–Pb_3O_4–ZnO–WO_3 glasses

Table 5 Mass attenuation coefficients of SiO_2–Pb_3O_4–ZnO–WO_3 glasses via FLUKA and XCOM

Energy (MeV)	G1			G2			G3		
	XCOM	FLUKA	Dev.%	XCOM	FLUKA	Dev.%	XCOM	FLUKA	Dev.%
0.6	0.11488	0.11405	0.718	0.11489	0.11383	0.923	0.11491	0.11419	0.619
1.25	0.05830	0.05788	0.727	0.05830	0.05792	0.648	0.05829	0.05794	0.606
1.5	0.05210	0.05174	0.685	0.05209	0.05172	0.724	0.05209	0.05170	0.742
2	0.04572	0.04548	0.530	0.04572	0.04552	0.443	0.04572	0.04556	0.346
3	0.04097	0.04079	0.433	0.04097	0.04080	0.436	0.04098	0.04077	0.518
5	0.03955	0.03944	0.284	0.03956	0.03942	0.373	0.03958	0.03944	0.353
10	0.04364	0.04350	0.309	0.04366	0.04358	0.190	0.04369	0.04358	0.254
Energy (MeV)	G4				G5				
	XCOM	FLUKA		Dev.%	XCOM	FLUKA		Dev.%	
0.6	0.11493	0.11418		0.649	0.11494	0.11408		0.751	
1.25	0.05828	0.05794		0.582	0.05827	0.05785		0.731	
1.5	0.05208	0.05169		0.735	0.05207	0.05176		0.599	
2	0.04571	0.04547		0.532	0.04571	0.04548		0.515	
3	0.04099	0.04077		0.524	0.04099	0.04074		0.614	
5	0.03960	0.03942		0.459	0.03961	0.03940		0.548	
10	0.04374	0.04359		0.341	0.04377	0.04349		0.632	

photon energy, whereas the μ values are higher than those of μ/ρ values. The important difference between μ/ρ and μ is that the μ factor is very helpful to understand the chemical composition dependence of the photon attenuation for the prepared glass specimens. For example, the curve of μ shows that the highest photon attenuation occurs by using G5 glass sample and the lowest photon attenuation occurs by using G1 glass samples. This indicates that the WO_3 addition plays an important role to attenuate the photons beam and then to improve the x/gamma shielding ability of the prepared glass system. More specifically, the maximum μ occurred at 0.6 MeV with the values of 0.728, 0.747, 0.759, 0.796, and 0.856 cm^{-1} for the prepared glass samples of G1, G2, G3, G4, and G5, respectively. The reason of such increase is the replacement of light metal oxide (ZnO) by higher one (WO_3). As WO_3 additive from 0 to 5 mol%, the LAC improved from 0.728 cm^{-1} to 0.856 cm^{-1}.

Therefore, it is recommended to increase the WO_3 content for getting more superior photon shielding properties of our designed glasses. Our simulation outcomes were numerically

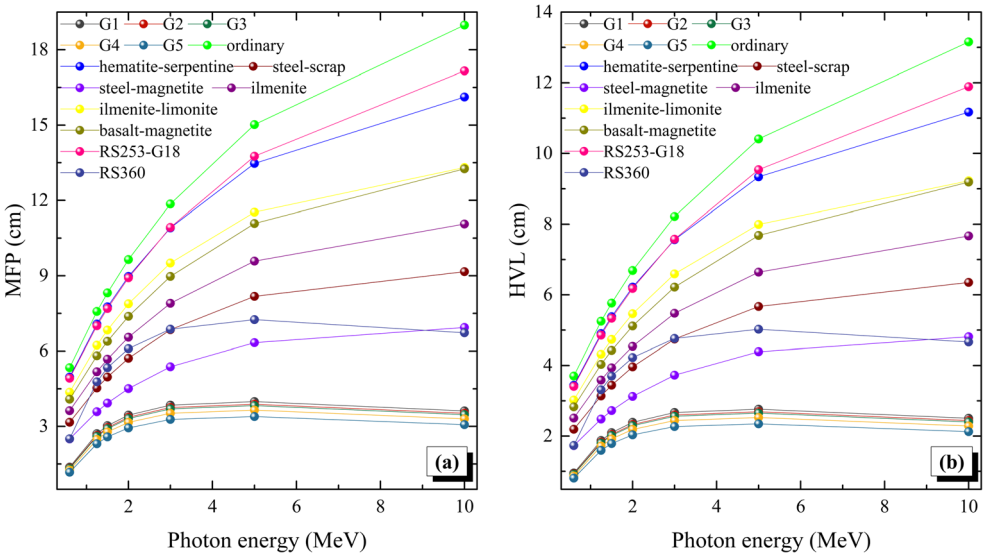

Fig. 10 MFP and HVL for the SiO_2–Pb_3O_4–ZnO–WO_3 glasses in contrast to other materials and commercial glasses

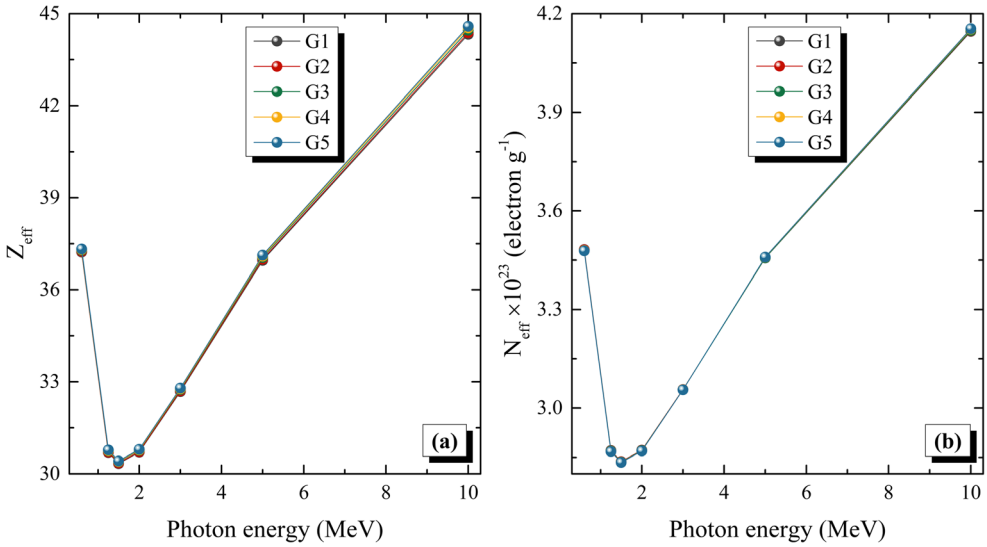

Fig. 11 Z_{eff} & N_{eff} for the SiO_2–Pb_3O_4–ZnO–WO_3 glasses

confirmed y using XCOM calculations for μ/ρ values. Table 5 listed all the values of μ/ρ obtained by FLUKA simulations and XCOM calculations for each glass sample over the entire considered energy range. Moreover, we listed the deviation (Dev. %) between the FLUKA & XCOM. The Dev. % values were estimated via the relation below:

$$\text{Dev.}(\%) = \frac{(\text{MAC})_{\text{XCOM}} - (\text{MAC})_{\text{FLUKA}}}{(\text{MAC})_{\text{XCOM}}} \times 100 \quad (3)$$

The highest Dev. % was noted at 1.25, 0.6, 1.5, 1.5, and 0.6 MeV with the values of 0.727, 0.923, 0.742, 0.735, and 0.751 for the glass samplings of G1 to G5, respectively. Therefore, the highest Dev. % between FLUKA and XCOM was observed for G2 glass sample with the value of 0.923. Such agreement confirms the accuracy of our simulation outcomes for all the studied parameters in the present work.

The previous interesting observations of the attenuation factors encouraged us taking more deep step to investigate the photon shielding capability of our present glass system. The transmission factors (MFP and HVL) are very important to choose a specific thickness of a material which uses for shielding applications. Moreover, they are usually used for comparing the photon shielding efficiency of new candidates with the conventional photon shields. Figure 10 shows a description for the photon shielding ability of our prepared glass system in terms of MFP and HVL as a comparison with several photon shields namely, ordinary, hematite-serpentine, ilmenite-limonite, basalt-magnetite, ilmenite, steel-scrap, and steel-magnetite concretes and commercial RS-253-G18 and RS360 glasses. Obviously, the MFP and HVL values are lower than those of traditional photon shields, indicating that our arranged glass (particularly G5) has superior shielding characteristics for x or gamma ray proposals. Another important factor in the photon attenuation studies is the effective atomic number (Z_{eff}) that is directly related to the partial interactions occurred at different energy regions. Furthermore, the Z_{eff} factor is a main term to determine the effective electron density (N_{eff}) of an absorbing medium. The calculated Z_{eff} & N_{eff} values were plotted as a function of energy for all of the prepared glass specimens as shown in Fig. 11. Obviously, the maximum of Z_{eff} & N_{eff} ($\times 10^{23}$ electron/g) occurred at energy of 10 MeV with the values of 44.326 & 4.146, 44.378 & 4.147, 44.455 & 4.148, 44.533 & 4.152, and 44.584 & 4.154 for the glass samples of G1, G2, G3, G4, and G5, respectively.

The final task in the present work is the evaluation of the energy absorption factors for each prepared glass sample. The first factor in this task is called specific gamma constant (SGC or Γ) that describes the radioactive source and its exposure in

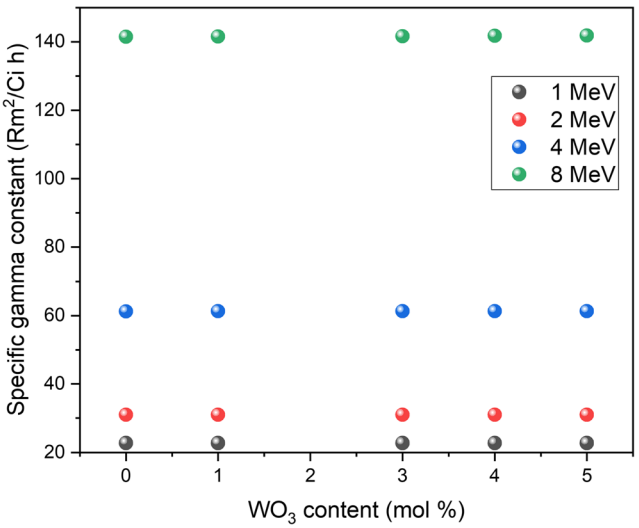

Fig. 12 Specific gamma ray constant for the SiO_2–Pb_3O_4–ZnO–WO_3 glasses at different photon energies (1, 2, 4, and 8 MeV)

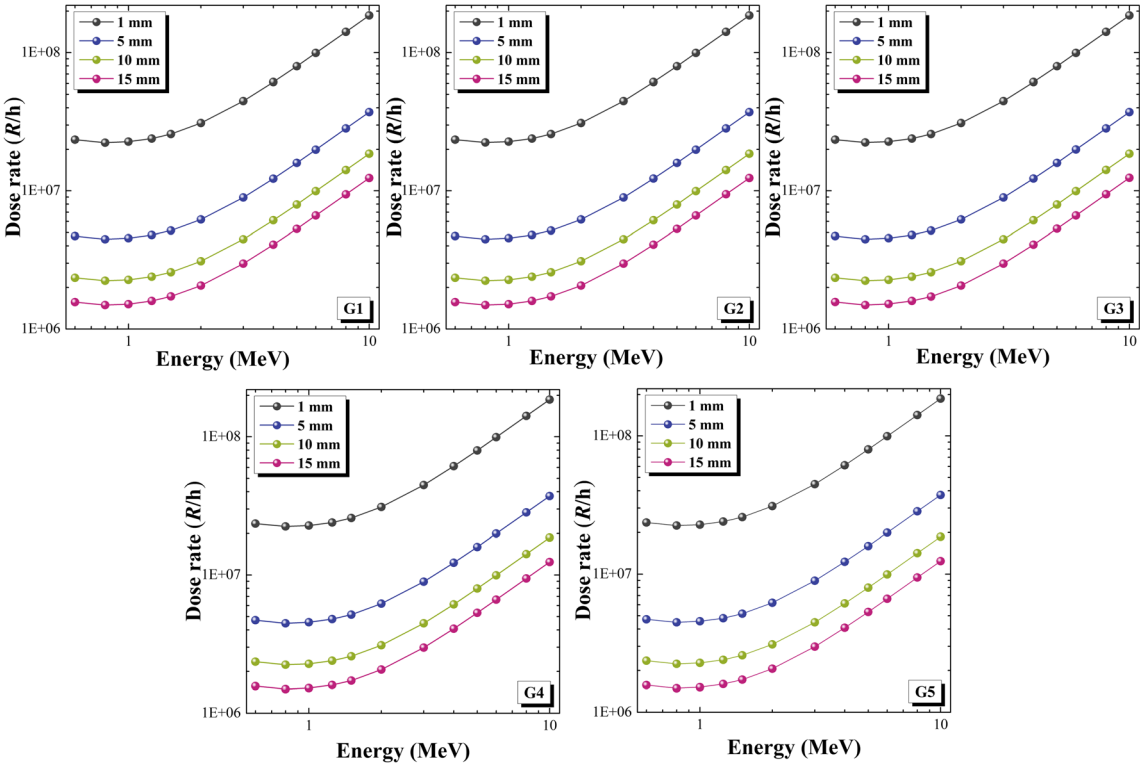

Fig. 13 Changes in gamma dose rate at varied energy for SiO_2–Pb_3O_4–ZnO–WO_3 glasses

air. The SGC values of the present prepared glass system were calculated and drawn as a function of WO_3 content for different photon energies namely, 1, 2, 4, and 8 MeV, as shown in Fig. 12. Clearly, the SGC has no significant change by increasing the concentration of WO_3 content at a given photon energy. However, there is a remarkable increase in the values of SGC as the photon energy. Such that the SGC factor increases from the value of about 61 Rm^2/ Ci h at 4 MeV to the value of about 141 Rm^2/ Ci h at 8 MeV. The second factor in this task is called mass energy absorption coefficient (MEAC) that measures the actual absorbed energy by a material (say glass sample). The MEAC factor is of importance in dose rate calculation that is a basic quantity for radiation applications in medicine. Both SGC and MEAC factors were used to calculate the dose rate for each prepared glass sample over the entire measured energy range. Figure 13 depicts the variation of dose rate (in unit of R/h) with photon energy at several levels of distance in the range between 1 and 15 mm. The values of the dose rate vary from the highest values at the lowest distance (e.g., 1 mm) to the lowest values at the highest distance (e.g., 15 mm). Moreover, one can notice that the rate of reduction in the dose rate was very large between 1 and 5 mm. At 0.6 MeV in the case of G5 glass (as an example), we found that the dose rate decreases from 2.35×10^7 R/h at 1 mm to 4.71×10^6 R/h at 4 mm.

4 Conclusions

Zinc lead silicate glass system contains different amount of WO_3 were fabricated with the traditional melt-quench technique. For these glasses, the physical, mechanical, and photon shielding parameters were investigated. The higher energy formation of W-O bonds than Zn-O is the main reason behind this conclusion which promotes the development of tungstate glasses rather than zincate. XRD result confirms the fabricated samples' amorphous nature. The parameters such as density, molar volume, and velocities (v_L and v_T) were measured and then used to determine the mechanical characterized of fabricated samples. Elastic moduli exhibits an increasing trend as WO_3 increases from 0 to 5 mol% and there is a good agreement between the experimental and theoretical elastic moduli. The maximum of Z_{eff} & N_{eff} ($\times 10^{23}$ electron/g) occurred at energy of 10 MeV with the values of 44.326 & 4.146, 44.378 & 4.147, 44.455 & 4.148, 44.533 & 4.152, and 44.584 & 4.154 for the glass samples of G1, G2, G3, G4, and G5, respectively. The WO_3 content plays an valuable role to attenuate the photons beam and then to improve the x/gamma shielding capability of the arranged glass system. The specific gamma constant (SGC) has no significant change by increasing the concentration of WO_3 content, while it swiftly increases from 61 Rm^2/ Ci h to 141 Rm^2/ Ci h as photon energy increases from 4 MeV to 8 MeV. It can be concluded that we successfully introduced a new glass system containing Pb_3O_4,

SiO_2, ZnO, and WO_3 with good mechanical properties and potential use in photon shielding applications.

Acknowledgments The authors extend their appreciation to the Deanship of Scientific Research at King Khalid University, Saudi Arabia for funding this work through Research Groups Program under grant number R.G.P.2/179/42. This work was also supported by Taif University Researchers Supporting Project number (TURSP-2020/63), Taif University, Taif, Saudi Arabia.

Funding Statement There are currently no Funding Sources on the list.

Author Contributions **Sultan Alomairy, Z.A. Alrowaili, and Imen Kebaili,** editing helping in reviewers' responses. **E.A. Abdel Wahab, C. Mutuwong, M.S. Al-Buriahi, and Kh. S. Shaaban,** Conceptualization, Methodology, Writing Reviewing Discussion and Editing helping in reviewers' responses.

Data Availability My manuscript and associated personal data.

Declarations

The manuscript has not been published.

Consent to Participate The authors consent to participate.

Consent for Publication The author's consent for publication.

Declaration of Competing Interest The authors declare that they have no known competing financial interests.

Conflict of Interest The authors declare that they have no conflict of interest.

References

1. Abdel Wahab EA, Shaaban KS, Yousef ES (2020) Enhancement of optical and mechanical properties of sodium silicate glasses using zirconia. Opt Quant Electron 52:458. https://doi.org/10.1007/s11082-020-02575-3
2. Shaaban K, Abdel Wahab EA, El-Maaref AA et al (2020) Judd–Ofelt analysis and physical properties of erbium modified cadmium lithium gadolinium silicate glasses. J Mater Sci Mater Electron 31:4986–4996. https://doi.org/10.1007/s10854-020-03065-8
3. E.A. Abdel Wahab, M.S.I. Koubisy, M.I. Sayyed, K.A. Mahmoud, A.F. Zatsepin, Sayed A. Makhlouf, Shaaban, Kh.S. (2021) Novel borosilicate glass system: $Na_2B_4O_7$-SiO_2-MnO_2 synthesis, average electronics polarizability, optical basicity, and gamma-ray shielding features, J Non-Crystalline Solids, \, 120509, https://doi.org/10.1016/j.jnoncrysol.2020.120509
4. El-Rehim AFA, Zahran HY, Yahia IS et al (2020) Physical, radiation shielding and crystallization properties of Na_2O-Bi_2O_3- MoO_3-B_2O_3- SiO_2 Fe_2O_3 glasses. Silicon. https://doi.org/10.1007/s12633-020-00827-1
5. El-Maaref AA, Abdel Wahab EA, Shaaban KS, El-Agmy RM (2021) Enhancement of spectroscopic parameters of Er^{3+}-doped cadmium lithium gadolinium silicate glasses as active medium for lasers and optical amplifiers in the NIR-region. Solid State Sci. https://doi.org/10.1016/j.solidstatesciences.2021.106539
6. Wahab EAA, Shaaban KS (2018) Effects of SnO_2 on spectroscopic properties of borosilicate glasses before and after plasma treatment and its mechanical properties. Mater Res Express 5(2):025207. https://doi.org/10.1088/2053-1591/aaaee8
7. Shaaban KS, Yousef ES, Abdel Wahab EA et al (2020) Investigation of crystallization and mechanical characteristics of glass and glass-ceramic with the compositions $x$$Fe_2O_3-35SiO_2-35B_2O_3-10Al_2O_3$-(20−$x$) Na_2O. J Materi Eng Perform. https://doi.org/10.1007/s11665-020-04969-6
8. Somaily HH, Shaaban KS, Makhlouf SA et al (2020) Comparative studies on polarizability, optical basicity and optical properties of Lead borosilicate modified with Titania. J Inorg Organomet Polym. https://doi.org/10.1007/s10904-020-01650-2
9. Saudi HA, Abd-Allah WM, Shaaban KS (2020) Investigation of gamma and neutron shielding parameters for borosilicate glasses doped europium oxide for the immobilization of radioactive waste. J Mater Sci Mater Electron 31(9):6963–6976. https://doi.org/10.1007/s10854-020-03261-6
10. Shaaban KS, Wahab EAA, Shaaban ER et al (2020) Electronic polarizability, optical basicity, thermal, mechanical and optical investigations of (65B_2O_3–30Li_2O–5Al_2O_3) glasses doped with Titanate. J Elec Materi 49:2040–2049. https://doi.org/10.1007/s11664-019-07889-x
11. Shaaban KS, Abo-Naf SM, Hassouna MEM (2019) Physical and structural properties of Lithium borate glasses containing MoO_3. Silicon 11:2421–2428. https://doi.org/10.1007/s12633-016-9519-4
12. Abdel Wahab EA, Shaaban KS, Elsaman R et al (2019) Radiation shielding, and physical properties of lead borate glass doped ZrO_2 nanoparticles. Appl Phys A Mater Sci Process 125:869. https://doi.org/10.1007/s00339-019-3166-8
13. Abd-Allah WM, Saudi HA, Shaaban KS et al (2019) Investigation of structural and radiation shielding properties of 40B_2O_3–30PbO–(30-x) BaO-x ZnO glass system. Appl Phys A Mater Sci Process 125:275. https://doi.org/10.1007/s00339-019-2574-0
14. Shaaban KS, Abo-naf SM, Abd Elnaeim AM, Hassouna MEM (2017) Studying effect of MoO_3 on elastic and crystallization behavior of lithium diborate glasses. Appl Phys A Mater Sci Process 123:6. https://doi.org/10.1007/s00339-017-1052-9
15. Shaaban KS, Koubisy MSI, Zahran HY et al (2020) Spectroscopic properties, electronic polarizability, and optical basicity of titanium–cadmium tellurite glasses doped with different amounts of lanthanum. J Inorg Organomet Polym. https://doi.org/10.1007/s10904-020-01640-4
16. Shaaban KS, Yousef ES, Mahmoud SA et al (2020) Mechanical, structural and crystallization properties in Titanate doped phosphate glasses. J Inorg Organomet Polym. https://doi.org/10.1007/s10904-020-01574-x
17. El-Maaref AA, Wahab EAA, Shaaban KS, Abdelawwad M, Koubisy MSI, Börcsök J, Yousef ES (2020) Visible and mid-infrared spectral emissions and radiative rates calculations of Tm^{3+} doped BBLC glass. Spectrochimica Acta Part A: Mol Biomol Spectros, 118774. https://doi.org/10.1016/j.saa.2020.118774
18. Shaaban KS, Zahran HY, Yahia IS et al (2020) Mechanical and radiation-shielding properties of B_2O_3–P_2O_5–Li_2O–MoO_3 glasses. Appl Phys A Mater Sci Process 126(10):804. https://doi.org/10.1007/s00339-020-03982-9
19. El-Sharkawy RM, Shaaban KS, Elsaman R, Allam EA, El-Taher A, Mahmoud ME (2020) Investigation of mechanical and radiation shielding characteristics of novel glass systems with the composition xNiO-20ZnO-60B_2O_3-(20-x) CdO based on nano metal oxides. J Non-Crystalline Solids 528:119754. https://doi.org/10.1016/j.jnoncrysol.2019.119754
20. El-Rehim AFA, Shaaban KS, Zahran HY et al (2020) Structural and mechanical properties of Lithium bismuth borate glasses containing molybdenum (LBBM) together with their glass–ceramics. J

Inorg Organomet Polym. https://doi.org/10.1007/s10904-020-01708-1
21. Shaaban KS, Wahab EAA, Shaaban ER et al (2020) Electronic polarizability, optical basicity and mechanical properties of aluminum lead phosphate glasses. Opt Quant Electron 52:125. https://doi.org/10.1007/s11082-020-2191-3
22. Shaaban KS, Yousef ES (2020) Optical properties of Bi_2O_3 doped boro tellurite glasses and glass ceramics. Optik - Int J Light Electron Optics 203:163976. https://doi.org/10.1016/j.ijleo.2019.163976
23. El-Rehim AA, Zahran H, Yahia I et al (2020) Radiation, crystallization, and physical properties of cadmium borate glasses. Silicon. https://doi.org/10.1007/s12633-020-00798-3
24. Abdel Wahab EA, El-Maaref AA, Shaaban KS, Börcsök J, Abdelawwad M (2020) Lithium cadmium phosphate glasses doped Sm^{3+} as a host material for near-IR laser applications. Optical Mater, 110638. https://doi.org/10.1016/j.optmat.2020.110638
25. AlBuriahi MS, Hegazy HH, Alresheedi F, Olarinoye IO, Algarni H, Tekin HO, Saudi HA (2020) Effect of CdO addition on photon, electron, and neutron attenuation properties of boro-tellurite glasses. Ceram Int. https://doi.org/10.1016/j.ceramint.2020.10.168
26. Abouhaswa AS, Mhareb MHA, Alalawi A, Al-Buriahi MS (2020) Physical, structural, optical, and radiation shielding properties of B_2O_3-20Bi_2O_3-20Na_2O_2-Sb_2O_3 glasses: role of Sb_2O_3. J Non-Crystalline Solids 543:120130. https://doi.org/10.1016/j.jnoncrysol.2020.120130
27. Naseer KA, Marimuthu K, Al-Buriahi MS, Alalawi A, Tekin HO (2020) Influence of Bi_2O_3 concentration on barium-telluro-borate glasses: physical, structural, and radiation-shielding properties. Ceram Int 47(1):329–340. https://doi.org/10.1016/j.ceramint.2020.08.138
28. Abouhaswa AS, Al-Buriahi MS, Chalermpon M et al (2020) Influence of ZrO_2 on gamma shielding properties of lead borate glasses. Appl Phys A Mater Sci Process 126:78. https://doi.org/10.1007/s00339-019-3264-7
29. Gokhan K, Agawany FIEL, Ilik BO, Mahmoud KA, Erkan I, Rammah YS (2021) Ta_2O_5 reinforced Bi_2O_3–TeO_2–ZnO glasses: fabrication, physical, structural characterization, and radiation shielding efficacy. Optical Mater 112:110757. https://doi.org/10.1016/j.optmat.2020.110757
30. Stalin S, Gaikwad DK, Al-Buriahi MS, Srinivasu C, Ahmed SA, Tekin HO, Rahman S (2020) Influence of Bi_2O_3/WO_3 substitution on the optical, mechanical, chemical durability and gamma ray shielding properties of lithium-borate glasses. Ceram Int. https://doi.org/10.1016/j.ceramint.2020.10.109
31. ElBatal HA, Abdelghany AM, ElBatal FH, EzzElDin FM (2012) Gamma rays interactions with WO_3-doped lead borate glasses. 134(1), 542 548. doi: https://doi.org/10.1016/j.matchemphys.2012.03.032
32. Kaur A, Khanna A, Sathe VG, Gonzalez F, Ortiz B (2013) Optical, thermal, and structural properties of Nb_2O_5–TeO_2 and WO_3–TeO_2 glasses. Phase Transit 86(6):598–619. https://doi.org/10.1080/01411594.2012.727998
33. ElBatal FH, Marzouk SY (2009) Interactions of gamma rays with tungsten-doped lead phosphate glasses. J Mater Sci 44:3061–3071. https://doi.org/10.1007/s10853-009-3406-y
34. Fayad AM, Ouis MA, ElBatal FH et al (2018) Shielding behavior of gamma-irradiated MoO_3 or WO_3-doped Lead phosphate glasses assessed by optical and FT infrared absorption spectral measurements. Silicon 10:1873–1879. https://doi.org/10.1007/s12633-017-9692-0
35. Alomairy S, Al-Buriahi MS, Abdel Wahab EA, Sriwunkum C, Shaaban K (2021) Synthesis, FTIR, and neutron/charged particle transmission properties of Pb_3O_4–SiO_2–ZnO–WO_3 glass system. Ceram Int 47:17322–17330. https://doi.org/10.1016/j.ceramint.2021.03.045
36. Makishima A, Mackenzie JD (1973) Direct calculation of Young's modulus of glass. J Non-Crystalline Solids 12(1):35–45. https://doi.org/10.1016/0022-3093(73)90053-7
37. Makishima A, Mackenzie JD (1975) Calculation of bulk modulus, shear modulus, and Poisson's ratio of glass. J Non-crystalline Solids 17(2):147–157. https://doi.org/10.1016/0022-3093(75)90047-2
38. Battistoni G, Cerutti F, Fasso A, Ferrari A, Muraro S, Ranft J, Roesler S, Sala PR (2007) The FLUKA code: Description and benchmarking." In AIP Conference proceedings, vol. 896, no. 1, pp. 31–49. American Institute of Physics
39. AlBuriahi MS, Hegazy HH, Faisal A, Olarinoye IO, Algarni H, Tekin HO, Saudi HA (2020) Effect of CdO addition on photon, electron, and neutron attenuation properties of boro-tellurite glasses. Ceram Int. https://doi.org/10.1016/j.ceramint.2020.10.168
40. Stalin S, Gaikwad DK, Al-Buriahi MS, Srinivasu C, Ahmed SA, Tekin HO, Rahman S (2020) Influence of Bi_2O_3/WO_3 substitution on the optical, mechanical, chemical durability and gamma ray shielding properties of lithium-borate glasses. Ceram Int. https://doi.org/10.1016/j.ceramint.2020.10.109
41. Al-Buriahi MS, Alajerami YSM, Abouhaswa AS, Alalawi A, Nutaro T, Tonguc B (2020) Effect of chromium oxide on the physical, optical, and radiation shielding properties of lead sodium borate glasses. J Non-Crystalline Solids 544:120171. https://doi.org/10.1016/j.jnoncrysol.2020.120171
42. Naseer KA, Marimuthu K, Al-Buriahi MS, Alalawi A, Tekin HO (2020) Influence of Bi_2O_3 concentration on barium-telluro-borate glasses: physical, structural and radiation-shielding properties. Ceram Int 47(1):329–340. https://doi.org/10.1016/j.ceramint.2020.08.138
43. Boukhris I, Imen K, Al-Buriahi MS, Amani A, Abouhaswa AS, Tonguc B (2020) Photon and electron attenuation parameters of phosphate and borate bioactive glasses by using Geant4 simulations. Ceram Int 46(15):24435–24442. https://doi.org/10.1016/j.ceramint.2020.06.226
44. Alothman MA, Alrowaili ZA, Alzahrani JS, Wahab EAA, Olarinoye IO, Sriwunkum C, Shaaban KS, Al-Buriahi MS (2021) Significant influence of MoO_3 content on synthesis, mechanical, and radiation shielding properties of B_2O_3-Pb_3O_4-Al_2O_3 glasses. J Alloys Compounds 882:160625. https://doi.org/10.1016/j.jallcom.2021.160625
45. Al-Buriahi MS, Singh VP, Alalawi A, Sriwunkum C, Tonguc BT (2020) Mechanical features and radiation shielding properties of TeO_2–Ag_2O-WO_3 glasses. Ceram Int. https://doi.org/10.1016/j.ceramint.2020.03.091